Bulletin de la Société Royale des Sciences de Liège, Vol. 80, 2011, p. 115 - 119

The Stellar Wind of LS 5039

Christina Aragona[1] , M. Virginia McSwain[1], and Mallory S. E. Roberts[2]

[1] Department of Physics, Lehigh University, USA
[2] Eureka Scientific, Inc., USA

Abstract: LS 5039 is an unusual high mass X-ray binary that also exhibits $\gamma-$ray emission modulated with its orbital period. The system consists of an ON6.5V((f)) star and an unidentified compact companion. Using the Australia Telescope Compact Array (ATCA), we have measured radio fluxes at 20cm, 13cm, 6cm, and 3cm between 2008 February and 2009 July. We have observed the Hα line with the Goodman High Throughput Spectrograph on the Southern Astrophysical Research (SOAR) telescope from 2010 June $2-4$. Here we combine these multiwavelength data to examine the structure of the massive star wind.

1 Introduction

LS 5039 is a member of the recently discovered class of γ-ray binaries. It consists of an ON6.5 V((f)) primary and an unidentified compact companion in a tightly bound, eccentric orbit with an orbital period of 3.906 days (McSwain et al. 2004; Casares et al. 2005; Aragona et al. 2009). The photosphere shows evidence of carbon depletion and nitrogen enrichment, indicating that mass transfer likely occurred between the O star and the supernova progenitor (McSwain et al. 2004). The system has a runaway velocity of 150 km s^{-1}, likely imparted by an asymmetric supernova explosion that occurred about 1.1 Myr ago (Ribó et al. 2002; McSwain et al. 2004).

The system has a low X-ray flux modulated with the orbital period and a hard spectrum (Bosch-Ramon et al. 2005; Takahashi et al. 2009). Both Fermi (energies between 100 MeV to 300 GeV) and HESS (energies above 0.1 TeV) have detected LS 5039 (Abdo et al. 2009; Aharonian et al. 2005, 2006). Both data sets confirm variability in the γ-ray emission modulated with the orbital period of the system.

Ribo et al. (2008) observed the system using the VLBA. Their two observations were spaced 5 days apart and showed a 12° change in the position angle of the system. Observations in the low-frequency radio regime, using the GMT, showed evidence of a spectral turnover at $\sim$ 964 MHz (Godambe et al. 2008). Bosch-Ramon (2009) used this collection of data to constrain a model of the radio emission sources in the system. He concludes that the low-frequency radio emission originates several AU from the primary star. Emission was also detected at 234 MHz.

In this work, we present observations of the Hα line taken with the Southern Astrophysical Research Telescope (SOAR) in order to probe the stellar wind of LS 5039. From this data set, we are able to derive a mass loss rate for the system and search for signs of changing wind morphology. We also present preliminary results from radio observations taken using the Australia Telescope Compact

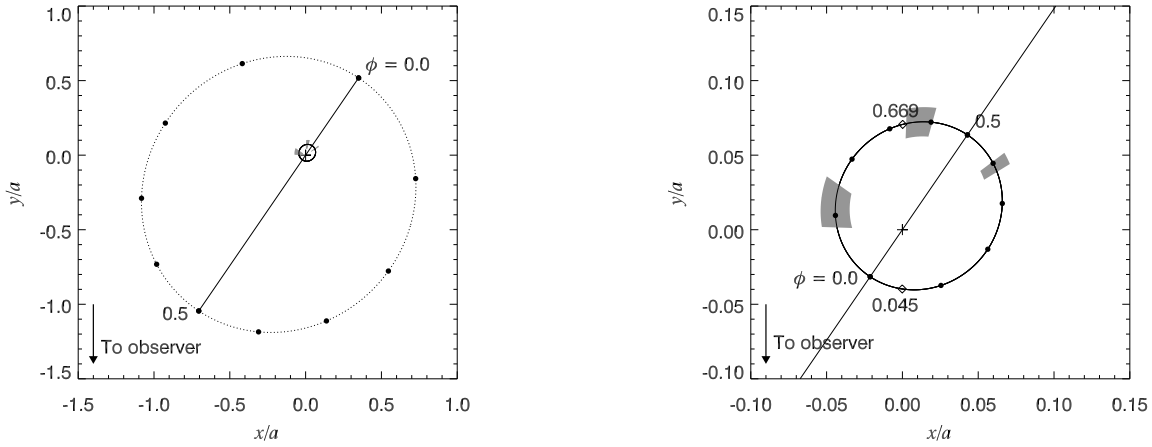

Figure 1: Left: the relative orbit of LS 5039 as seen from above. The black circles mark intervals of 0.1 phase. The dotted line represents the orbit of the compact object, which we assumed to have a mass of 1.4 $M_\odot$. The solid line represents the orbit of the O star, assumed to have a mass of 23 $M_\odot$ (Casares et al. 2005). Right: a close up view of the O star orbit, to highlight the orientation of the system during our SOAR observations. The gray shaded regions indicate the phases of our observations. The diamonds mark the phases of inferior and superior conjunction.

Array (ATCA). We compare these flux measurements with the expected thermal radio emission, calculated using the mass loss rates obtained from the Hα equivalent width, to confirm the fraction of the total radio emission due to non-thermal processes.

2 Observations

2.1 Optical

We observed LS 5039 using the Goodman High Throughput Spectrograph (GHTS) on SOAR from 2–4 June 2010. We used the 1200 l/mm grating in 1^{st} order to obtain a wavelength range of 5550–6850 Å and a resolving power, $R = \lambda/\delta\lambda$ = 6000–7000. Exposure times ranged from 10 to 15 minutes in duration. A flat field and a Ne comparison lamp spectrum were taken after each exposure, and spectra were zero-corrected, flatfielded, and wavelength calibrated using standard procedures in IRAF[1]. Our observations were taken between orbital phases 0.38–0.92 (see Figure 1, right), calculated using the orbital ephemeris from Aragona et al. (2009).

2.2 Radio

Radio observations were taken using the Australia Telescope Compact Array (ATCA) between 2008 February and 2009 July. Each observation spanned a 2–3 hour period. We switched between the 3cm/6cm back end and 13cm/20cm back end 2–3 times over each observation to ensure that the mid-exposure times at each wavelength were approximately the same. Data were reduced using standard procedures in MIRIAD. We defined the location of bright sources in our field and used the CLEAN algorithm to model the observed radio flux in each wavelength band. After five iterations of cleaning

[1]IRAF is distributed by the National Optical Astronomy Observatory, which is operated by the Association of Universities for Research in Astronomy, Inc., under cooperative agreement with the National Sciences Foundation

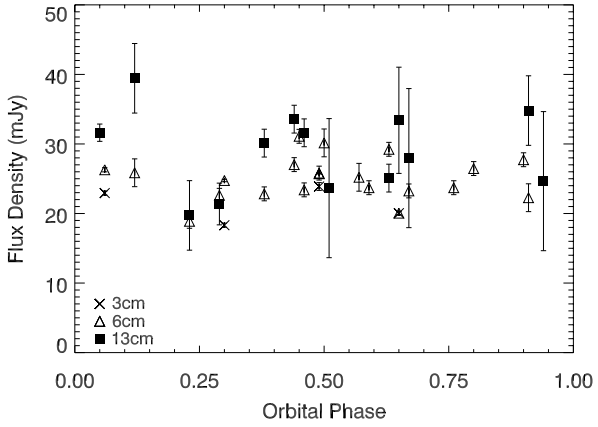

Figure 2: Radio flux measurements of LS 5039.

and self calibration, we used the *imfit* module to measure the flux from LS 5039. The results for the 3cm, 6cm, and 13cm data are plotted in Figure 2. The 20cm fluxes are still being reduced.

3 Hα Equivalent Widths and Mass Loss Rates

We coadded the spectra from SOAR in sets of two to improve the signal-to-noise, S/N, of the data and used the orbital ephemeris of Aragona et al. (2009) to shift the Hα line in each observation to the rest wavelength. Casares et al. (2005) noted blue-shifted points in their radial velocity data at phase 0.45. The radial velocity curved used to determine the orbital parameters in Aragona et al. (2009) showed additional blue-shifted points between phases 0.4 and 0.6. To investigate the source of these spurious points, we examined Hα for changing line profiles which would indicate the presence of large scale structures in the wind (such as a focused wind stream). The resulting plot is shown in Figure 3. The line profile does not show variation above the level of the noise.

We also determined the mass loss rate of the system (Figure 4) from the equivalent width of the Hα line, $W_{H\alpha}$, using the method of Puls et al. (1996) and assuming a β=1 velocity law. The measurements show considerable scatter but no significant variation correlated with orbital phase. We find an average mass loss rate of 1.9 x 10^{-8} $M_\odot$ yr^{-1}. Spectra from the Goodman spectrograph suffer from fringing near the Hα line. Thus far, we have not corrected for this effect. Once we correct for fringing, we will reexamine these spectra for small variations in the line profile which might indicate large scale structure in the wind.

4 Radio Emission from the Stellar Wind

Our preliminary optical results justify assuming a spherically symmetric stellar wind when modeling the radio emission. We calculated the free-free opacity due to ionized electrons in the wind and determined the optical depth, τ_ν, of the wind as a function of stellar distance using the method outlined in Lamers and Cassinelli (1999). The free-free optical depth is

$$\tau_\nu = 1.13 \times 10^{-4} \frac{g_\nu}{\mu^2} \nu^{-2} R^{-3/2} \left(\frac{\dot{M}}{v_\infty}\right)^2 R_\star^{-3} \int_r^\infty x^{-4} w^{-2} dr \qquad (1)$$

where μ is the mean atomic mass, ν is the frequency, g_ν is the gaunt factor, T is the temperature of the wind, $\dot{M}$ is the mass loss rate, v_∞ is the terminal wind velocity, $R_\star$ is the radius of the star, w is

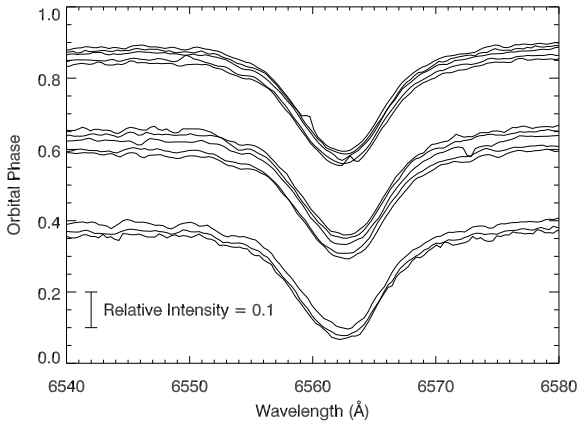

Figure 3: The Hα line from the SOAR observations. Consecutive pairs of spectra were coadded to improve S/N. We shifted each spectrum to the rest wavelength to highlight any variations in the line profile due to structure in the stellar wind.

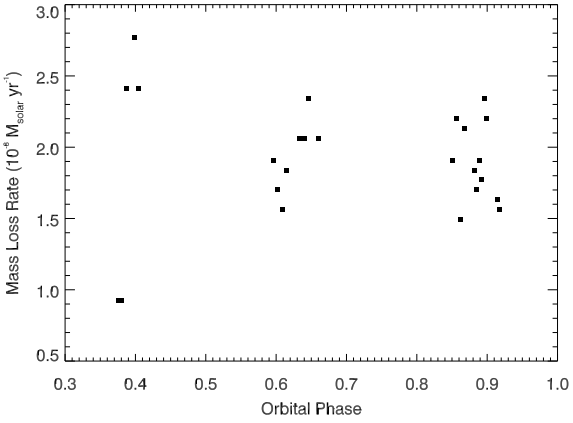

Figure 4: The mass loss rate of LS 5039 plotted as a function of orbital phase. We estimate an error of 0.5×10^{-8} $M_\odot$ yr^{-1} originating from measuring $W_{H\alpha}$ rather than any real variation in the mass loss rate of the system over the orbital period.

Table 1: Radio flux expected from a thermally emitting stellar wind compared to our measured fluxes.

λ (cm)	20	13	6	3
R(τ_ν = 1/3) ($R_\odot$)	223.3	167.4	102.3	65.1
$F_{predicted}$ (mJy)	0.00008	0.0002	0.0009	0.0034
$\langle F_{observed} \rangle$ (mJy)	–	29.0	25.0	21.3

the wind velocity divided by v_∞, and x is the distance from the star divided by $R_\star$. We assumed a fully ionized hydrogen wind following a β=1 velocity law. All values are in cgs units.

We calculated the distance from the star at which τ_ν=1/3, where the stellar wind becomes opaque to radio waves. We assumed that the wind would emit as a blackbody at this radius and used the Rayleigh-Jeans approximation to estimate the resulting radio flux predicted at 3cm, 6cm, 13cm, and 20cm. The results are shown in Table 1. The calculated radio flux expected from a thermally emitting stellar wind is on the order of μJy for each wavelength band. By contrast, our radio observations (Figure 2) show fluxes on the order of 10–40 mJy. Clearly the bulk of the radio flux in this system is not due to a thermally emitting stellar wind.

We performed a preliminary calculation of the spectral index using pairs of 3cm/6cm and 6cm/13cm fluxes that were observed simultaneously. Purely thermal radio emission from the stellar wind should have a spectral index, Γ, of -0.6, where $F_\nu \alpha \nu^{-\Gamma}$. For the 6cm/13cm points, values for α lie between 0.5 and -1.0, have error bars larger than the scatter in the points, and show no obvious trends with respect to orbital phase. For the 3cm/6cm fluxes, the values are between -0.2 and 0.6. However, the 3cm data set has proven more problematic to reduce, resulting in fewer reliable flux measurements at the time of these calculations. Consequently, we cannot draw any conclusions about the source of the emission at this time. We hope that improving the error bars on the observed radio fluxes and adding the 20cm data points will allow us to achieve better results in the future.

5 Conclusion

The error bars on the radio observations are fairly large, but there appears to be real variation in radio emission with respect to orbital phase, particularly between phase 0.0 and phase 0.25. The observed radio flux variations cannot be explained by pure free-free emission produced in the stellar wind of the primary, as this should be constant with respect to orbital phase. The emission is probably generated by the interaction between the stellar wind and the compact object. The correlation of the radio emission with orbital phase suggests a wind-wind interaction region: the variations in radio emission produced by a precessing jet should not depend on orbital phase. In the colliding wind scenario, a non-thermal distribution of particles is ejected into the shock region from the relativistic pulsar wind. This material will flow away from the shock region in a comet like tail, with emission dominated by synchotron losses. The radio emission expected from such a scenario would be modulated with orbital phase (Dubus 2006). Furthermore, a radio map of such a configuration would bear some resemblance to a microquasar jet (Dubus 2006), which is consistent with the observations of Paredes et al. (2000).

Due to the different optical depths for radio waves and Hα, we can assume that our observations probe two different regions of the stellar wind, with the Hα line carrying information about the wind closer to the star. Future work will include more detailed modeling of the interaction between the neutron star and the stellar wind.

Acknowledgements

We are grateful for support from NASA DPR Nos. NNX 08AV70G, NNX 09AT67G, and Lehigh University. We would like to thank Sean Points for aiding us with the use of the SOAR GHTS and data reduction, and P. Edwards and R. Wark for scheduling and aid in taking observations with ATCA.

References

Abdo, A. A., Ackermann, M., Ajello, M., Atwood, W. B., Axelsson, M., Baldini, L., Ballet, J., Barbiellini, G., et al. 2009, ApJ, 706, L56

Aharonian, F., Akhperjanian, A. G., Aye, K.-M., Bazer-Bachi, A. R., Beilicke, M., Benbow, W., Berge, D., Berghaus, P., et al. 2005, Science, 309, 746

Aharonian, F., Akhperjanian, A. G., Bazer-Bachi, A. R., Beilicke, M., Benbow, W., Berge, D., Bernlöhr, K., Boisson, C., et al. 2006, A&A, 460, 743

Aragona, C., McSwain, M. V., Grundstrom, E. D., Marsh, A. N., Roettenbacher, R. M., Hessler, K. M., Boyajian, T. S., & Ray, P. S. 2009, ApJ, 698, 514

Bosch-Ramon, V. 2009, A&A, 493, 829

Bosch-Ramon, V., Paredes, J. M., Ribó, Miller, J. M., Reig, P., & Martí, J. 2005, ApJ, 628, 388

Casares, J., Ribó, M., Ribas, I., Paredes, J. M., Martí, J., & Herrero, A. 2005, MNRAS, 364, 899

Dubus, G. 2006, A&A, 456, 801

Godambe, S., Bhattacharyya, S., Bhatt, N., & Choudhury, M. 2008, MNRAS, 390, L43

Lamers, H. J. G. L. M., & Cassinelli, J. P., 1999, *Introduction to Stellar Winds* (New York, NY: Cambridge University Press)

McSwain, M. V., Gies, D. R., Huang, W., Wiita, P. J., Wingert, D. W., & Kaper, L. 2004, ApJ, 600, 927

Paredes, J. M., Martí, J., Ribó, M., & Massi, M. 2000, Science, 288, 2340

Puls, J., Kudritzki, R.-P., Herrero, A., Pauldrach, A. W. A., Haser, S. M., Lennon, D. J., Gabler, R., Voels, S. A., et al. 1996, A&A, 305, 171

Ribó, M., Paredes, J. M., Moldón, J., Martí, J., & Massi, M. 2008, A&A, 481, 17

Ribó, M., Paredes, J. M., Romero, G. E., Benaglia, P., Martí, J., Fors, O., & García-Sánchez, J. 2002, A&A, 384, 954

Takahashi, T., Kishishita, T., Yasunobu, U, Tanaka, T., Yamaoka, K., Khangulyan, D., Aharonian, F. A., Bosch-Ramon, V., et al. 2009, ApJ, 697, 592